Send Orders for Reprints to reprints@benthamscience.net

612 *Current Nanoscience,* **2023,** ***19,*** **612-619**

RESEARCH ARTICLE

Carbon Nanodots/Cajuput Oil Composites for Potential Antibacterial Applications

Ariswan Ariswan[1], Isnaeni Isnaeni[2], Warsono Warsono[1], Fika Fauzi[1], Irvany Nurita Pebriana[1], Suparno Suparno[1], Emi Kurnia Sari[3], Bian Itsna Ashfa Al Ashfiya[1] and Wipsar Sunu Brams Dwandaru[*1]

[1]*Department of Physics Education, Faculty of Mathematics and Natural Sciences, Universitas Negeri Yogyakarta, Jalan Colombo No 1, Karangmalang, Yogyakarta 55281, Indonesia;* [2]*Research Centre of Physics, Indonesia Institute of Sciences, Banten 15314, Indonesia;* [3]*Department of Physics, Faculty of Mathematics and Natural Sciences, Universitas Gadjah Mada, Sekip Utara, Bulaksumur, Yogyakarta 55281, Indonesia*

ARTICLE HISTORY

Received: May 15, 2022
Revised: August 20, 2022
Accepted: September 18, 2022

DOI:
10.2174/1573413719666221114094255

Abstract: ***Background*****:** We reported for the first time the preparation of carbon nanodots/cajuput oil (C-dots/CJO) composites for potential antibacterial applications.

Methods**:** The C-dots were synthesized from CJO distillation wastes *via* the low carbonization method. Then, the C-dots were mixed with CJO to obtain C-dots/CJO composites. The characteristics of the C-dots were determined using UV-Vis, PL, TRPL, FTIR, and HRTEM, whereas the C-dots/CJO composites were characterized using UV-Vis and FTIR.

Results**:** Antibacterial properties were investigated for samples of C-dots, CJO, and C-dots/CJO with no-light, white light, and UV/violet light treatments. The C-dots produced cyan luminescence with a decay lifetime of 6.54 ns. Based on the antibacterial tests, the C-dots/CJO composites have DIZ higher than the pure C-dots.

Conclusion**:** The C-dots/CJO composites reached the highest DIZ of 3.6 nm under white light, which was attributed to the photodynamic effect and photodisinfection of the C-dots and CJO, respectively. Hence, the C-dots/CJO composites can be potential antibacterial agents against *E. coli* bacteria.

Keywords: Antibacterial activity, C-dots/CJO composites, carbon nanodots, cajuput oil, low carbonization method, cajuput oil distillation wastes.

1. INTRODUCTION

Microorganisms, such as bacteria, can be a threat to human health. Bacteria can enter our body through various surfaces, e.g., food and water [1,2]. Pathogenic bacterial infections and their uncontrolled proliferation can cause serious illnesses in humans, such as tuberculosis, cholera, and meningitis. However, some bacteria are resistant to the existing conventional antibiotics, *e.g.*, methicillin-resistant *Staphylococcus aureus* (MRSA), vancomycin-resistant *Enterococcus faecium* (VRE), and *Streptococcus pneumoniae* [3,4]. Therefore, antibacterial technology that is more effective in suppressing and fighting bacterial growth is needed. Presently, nanotechnology is taking center stage in the development of antibacterial agents, *e.g.*, carbon nanodots (C-dots) and graphene quantum dots (GQDs) [3,5,6].

*Address correspondence to this author at the Department of Physics Education, Faculty of Mathematics and Natural Sciences, Universitas Negeri Yogyakarta, 55281, Yogyakarta Indonesia; Tel: +62 878 396 364 16;
E-mail: wipsarian@uny.ac.id

C-dots are zero-dimensional (0D) nanoparticles having diameters from 1 nm to 10 nm, which consist of core and surface states [7]. The core consists of sp^2 or sp^3 carbon structures, which show graphitic or amorphous carbon forms [8]. On the other hand, the surface state consists of functional groups or polymers, such as carboxyl, hydroxyl, and amines, which can provide good solubility properties so that they are easily combined with other materials [9]. C-dots have other excellent properties, such as strong absorption in UV regions, high luminescence, good biocompatibility, and non-toxicity [4,10,11]. The properties produced by C-dots depend on the synthesis method and the precursors used. The preparation of C-dots can be carried out by electrochemical methods, hydrothermal treatment, microwave-assisted, and low-temperature carbonization [11-15]. In addition, various precursors, such as watermelon peel, granulated sugar, and spinach, have been successfully prepared into C-dots [11,15,16].

Facile synthesis and various excellent properties have made C-dots continue to be developed and applied in various

1573-4137/23 $65.00+.00

fields, such as bio-imaging, biosensors, drug delivery, and antibacterial agents [3,6,8]. For antibacterial application, C-dots are combined with other substances to form composites. C-dots composites produced are C-dots with antimicrobial reagents, *e.g.*, H_2O_2, Na_2CO_3, and AcOH, C-dots with antibiotic ciprofloxacin, and a combination of C-dots with antibacterial quaternary ammonium compound lauryl betaine (BS-12). These combinations can increase the inhibition effectiveness against *Escherichia coli* (*E. coli*) bacteria [3,6,17]. Hence, the antibacterial properties of C-dots are stronger and more effective when combined with other antibacterial agents, known as synergistic activity against bacteria [18]. In addition, the antibacterial properties are also influenced by the concentration of the C-dots solution. Another advantage based on the excellent luminescence property of C-dots is their photodynamic effect. This latter property may be used for strengthening the antibacterial activity of the C-dots [19].

Natural antibacterial substances that can resist the growth of microorganisms in living tissue (antiseptic) are phenolic crystals, which can be found in cajuput oil (CJO) [20]. Apart from phenolics, CJO contains other chemical compounds, such as monoterpene, linalool, terpinene, terpineol, and cineol, which also have antibacterial properties. The kinetics of the antibacterial activity of CJO against *E. coli*, *Bacillus cereus*, and *S. aureus* has been studied by determining the reaction orders [21]. The antibacterial activity of CJO has also been studied against aflatoxigenic strains of *Aspergillus flavus* for food preservative applications [22]. Moreover, CJO has been used as an external topical medicine, such as a reliever for itching and fever [23].

CJO is obtained through the distillation process of the leaves and stems of the cajuputi (*Melaleuca cajuputi*) plant. The CJO distillation process is shown in Fig. (**1**). Hence, the high consumption of CJO causes an increase in leaf and stem wastes of CJO distillation [24], as indicated by the red arrows in Fig. (**1**). The solid waste is usually used as fertilizer or dumped because it is no longer used. Furthermore, liquid waste is also produced in the distillation process, as indicated by the blue arrow in Fig. (**1**). Therefore, in this study, we propose a method of processing this solid waste into functional materials, *i.e.*, C-dots. In addition, the resulting C-dots could be combined with CJO-producing C-dots/CJO composite to enhance the antibacterial activity of C-dots.

In this study, we report the preparation and characterizations of C-dots/CJO composites for potential antibacterial applications. As per our knowledge, the combination of C-dots and CJO has not been explored so far. The characteristics of the C-dots and C-dots/CJO composites are determined by means of ultraviolet-visible (UV-Vis) spectroscopy and Fourier transform infrared (FTIR), whereas the C-dots are further characterized using photoluminescence (PL), time-resolved photoluminescence (TRPL), and high-resolution transmission electron microscopy (HRTEM). The antibacterial properties of the C-dots/CJO composites are tested against *E. coli* bacteria by the diffusion method treated with no light, white light, and UV/violet light. The antibacterial activity is indicated by the diameter of the inhibition zone (DIZ) of the samples.

2. MATERIALS

The wastes were obtained from a local CJO factory in Yogyakarta, Indonesia. This factory processes cajuput plants by utilizing 18 tons of fresh twigs and leaves to become CJO through a distillation process. This distillation process produces solid (red arrows in Fig. (**1**)) and liquid (blue arrows in Fig. (**1**)) wastes. The instruments used for characterizations were UV-Vis spectrophotometer Shimadzu UV-Vis 2450, FTIR Thermo Nicolet Avatar 360 IR, HRTEM model FEI Tecnai G2 F20 200 kV, PL, and TRPL. The PL and TRPL MayP112615 Spectrum 2068 used a picosecond 420 nm laser from PicoQuant, a MAYAPro2000 spectrometer from Ocean Optics, and TCSPC PicoHarp 260 photon detector from PicoQuant.

The source of the white light and UV/violet light was a portable light emitting diode (LED) UV blacklight flashlight with 11.7 cm in length, 16 cm in diameter, and a power of 5 W. Finally, the *E. coli* bacteria was purchased from the Medical Faculty of Universitas Gadjah Mada, Indonesia.

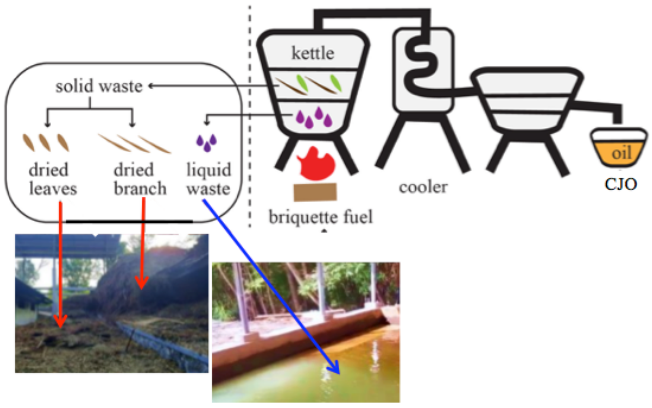

Fig. (1). The CJO distillation process producing solid and liquid wastes. (*A higher resolution / colour version of this figure is available in the electronic copy of the article*).

3. EXPERIMENTAL SECTION

The solid wastes from the CJO distillation process were sorted out since only the leftover cajuput leaves would be used for the C-dots production. The leaves were dried for a few days in the sun and then pounded into powder. The powder was then carbonized at 230 °C for 60 minutes in an oven. Afterward, the powder was further ground in order to get a very fine powder. Then, 3.0 g of the powder was dissolved in 100 mL of deionized (DI) water and stored for four days. Finally, the mixture was filtered using filter papers with a diameter of 110 μm in order to obtain the C-dots dispersion.

The C-dots dispersion was mixed with CJO and Tween 80. The volume ratio of C-dots, CJO, and Tween 80 was 3: 1: 1. The mixture was then heated at 40 °C and stirred for 10 minutes until it became homogenous. Hence, the C-dots/CJO composites were obtained.

The C-dot samples were characterized by means of UV-Vis, PL, TRPL, FTIR, and HRTEM. Furthermore, the C-

dots/CJO sample was characterized using UV-Vis and FTIR. The Shimadzu UV-Vis 2450 spectrophotometer was employed to determine the C-dots and C-dots/CJO composites absorption spectra. The PL and TRPL tests were carried out to determine the emission wavelength and electronic decay lifetime of the C-dots, respectively. The PL and TRPL spectra were recorded by an avalanche photodiode controlled by Picohard260 software. For this measurement, we used a pulsed laser with a fast 40 MHz repetition rate. The FEI Tecnai G2 F20, 200 kV HRTEM, having a resolution of 0.16 nm with carbon coated 300 mesh copper grid, was utilized to determine the average diameter of the C-dots. The FTIR Thermo Nicolet Avatar 360 IR was used to determine the functional groups in the C-dots and C-dots/CJO composite samples.

The antibacterial activities of C-dots, CJO, and C-dots/CJO composites toward *E. coli* were measured using the diffusion method. In the first stage, the bacterial culture was grown in nutrient agar (NA) and nutrient Broth (NB) media. The bacteria were then cultured in a medium on a petri dish. Afterward, paper discs were immersed in the samples for 15 minutes. After soaking, the paper discs were placed on the solidified NA media and were put in a sterile room at 37 ^{o}C.

Three petri dishes were then given different treatments, *i.e.*, one petri dish was put in a dark location (no light), and the other two petri dishes were exposed to white light and UV/violet light, respectively. The antibacterial activity of the samples was determined by the DIZ formed by each sample, *i.e.*, C-dots, CJO, and C-dots/CJO composites. The DIZ measurements were carried out three times for each sample using a caliper, then the mean DIZ was determined. These measurements were taken every three hours for 24 hours. The results were analyzed to determine the DIZ in preventing the growth of *E. coli*.

4. RESULTS AND DISCUSSION

The absorption and luminescence characteristics of the C-dots sample are shown in Fig. (**2**). It can be observed that C-dots have one absorption peak at 214 nm and a low shouldering peak at 280 nm. The absorption peaks at 214 nm and 280 nm show electronic transitions of $\pi \rightarrow \pi^*$ of the C=C functional group [10,25]. Moreover, the PL spectrum of the C-dots sample shows an emission peak at 515 nm, which then broadens in the range of 500 nm - 570 nm, indicating cyan luminescence, as shown in the right-inset of Fig. (**2**) [6,11,15,26].

Another verification of the existence of C-dots is provided by the TRPL spectrum given in Fig. (**3**). The spectrum shows the decay lifetime of the C-dots excited by a picosecond laser at 420 nm. This decay lifetime shows the amount of time for electrons to move back from the π or surface state to the highest occupied molecular orbital (HOMO) [27]. The TRPL spectrum (blue graph in Fig. (**3**)) is the observed decay lifetime of the C-dots sample, which is a very short time duration, *i.e.*, 25 ns. The TRPL spectrum was then fitted using multi-exponential decay, which started from 2.375 nm until 25.00 nm. The result shows that the decay lifetime of the C-dots is 6.54 ns, which is a typical decay lifetime for a fluorescent material, such as C-dots.

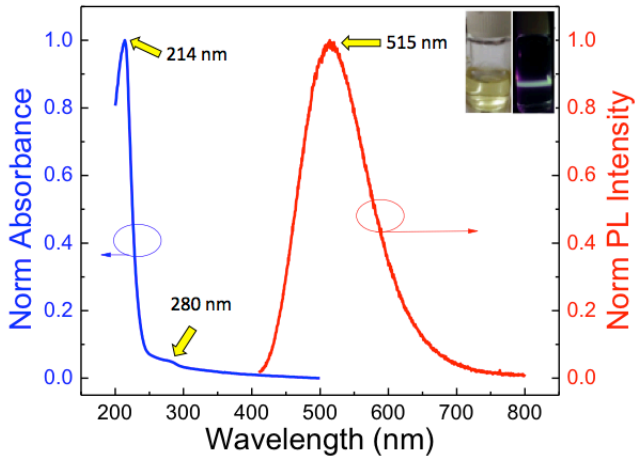

Fig. (2). Absorption and luminescence spectra of the C-dots. (*A higher resolution / colour version of this figure is available in the electronic copy of the article*).

Furthermore, the functional groups contained in the C-dots sample can be identified using the FTIR spectrum, as shown in Fig. (**4**). It can be observed that there are three functional groups contained in the C-dots sample, namely C=C at 1635.43 cm^{-1}, C-H at 2065.49 cm^{-1}, and O-H at 3438.63 cm^{-1}. The C=C functional group indicates the core of C-dots, while C-H and O-H functional groups designate the surface state of the C-dots [28,29].

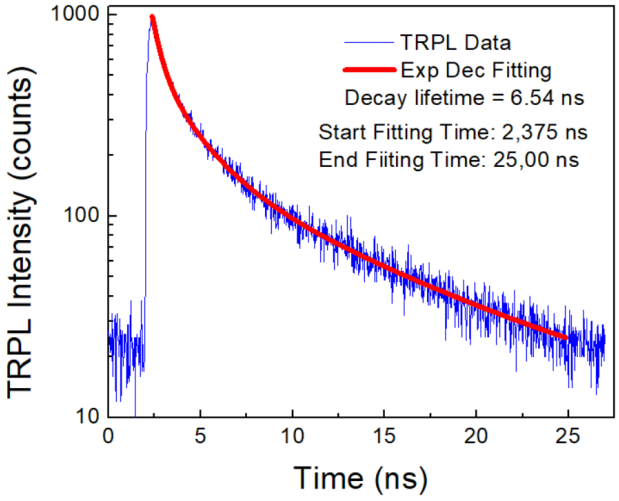

Fig. (3). The decay lifetime of the C-dots sample. (*A higher resolution / colour version of this figure is available in the electronic copy of the article*).

The size of the C-dots sample is determined from the HRTEM image, as shown in Fig. (**5a**-left). The C-dots are indicated by the black spots on the figure (the yellow arrow). Moreover, it can also be seen that the C-dots are not evenly distributed in the sample. The histogram distribution of the C-dots diameters is shown in Fig. (**5b**-right). The figure shows that the mean C-dot diameter is 2.88 nm. Furthermore, the average diameter of the C-dots is 2.9 nm, which is a typical diameter of C-dots, *i.e.*, between 1 nm to 10 nm [30].

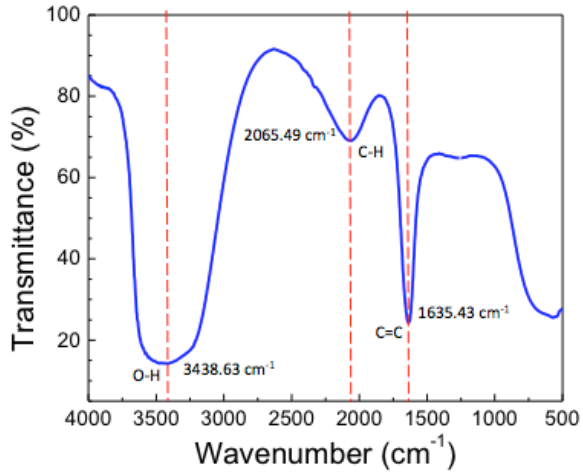

Fig. (4). IR spectrum of the C-dots. (*A higher resolution / colour version of this figure is available in the electronic copy of the article*).

The C-dots/CJO composite consisted of a yellowish color solution, as shown in the inset of Fig. (**6**). Moreover, compared to the pure C-dots in Fig. (**2**), the C-dots/CJO solution is murkier, due to the addition of the CJO. To verify the formation of C-dots/CJO composite, the UV-Vis and FTIR characterizations were performed. A comparison of the UV-Vis spectra of C-dots, C-dots/CJO composites, and CJO samples can be seen in Fig. (**6**). It can be seen that the pure C-dots spectrum is different from both CJO and C-dots/CJO composite spectra. The pure C-dots spectrum has one absorption peak and one shouldering peak, whereas CJO and C-dots/CJO samples have two absorption peaks and one shouldering peak, respectively. The C-dots/CJO composite spectrum is similar to that of CJO but exhibits shifts in its absorption peaks.

The C-dots, C-dots/CJO, and CJO samples exhibit the first absorption peaks at 214 nm, 232 nm, and 234 nm, respectively. As previously explained, the peak at 214 nm indicates the existence of the core of C-dots. For CJO, the absorption peak at 234 nm indicates an electronic transition of the -CHO bond, which is an aromatic compound of benzaldehyde. It is known that benzaldehyde is one of the compounds in CJO. The first absorption peak of the C-dots/CJO composite is between the first peaks of CJO and C-dots spectra, which means that the first peak of the C-dots/CJO composite contains the absorption characteristics of the C-dots and CJO, *i.e.*, an electronic transition of the C=C bond [31].

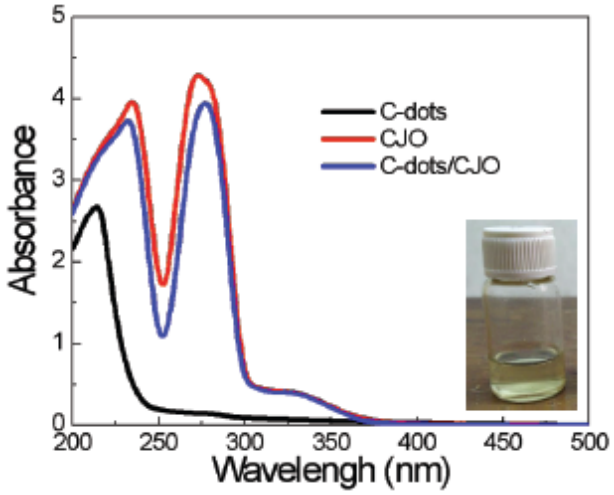

Fig. (6). Absorption spectra of the C-dots, CJO, and C-dots/CJO composites. (*A higher resolution / colour version of this figure is available in the electronic copy of the article*).

The second absorption peaks for the C-dots/CJO and CJO samples appear at 272.5 nm and 274 nm, respectively.

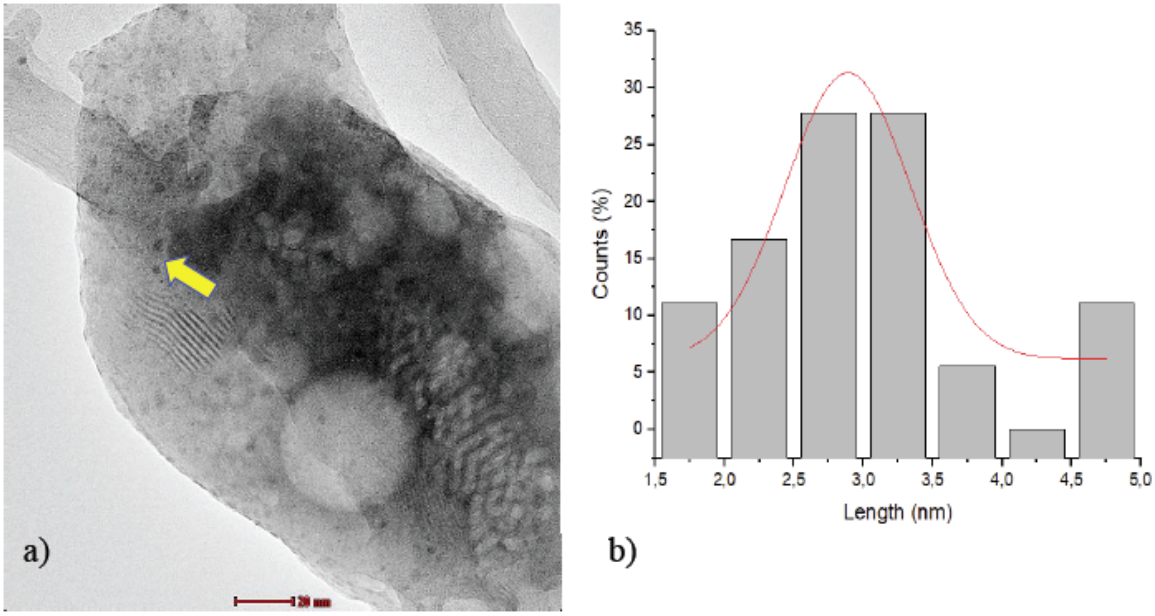

Fig. (5). C-dots images using HRTEM. (*A higher resolution / colour version of this figure is available in the electronic copy of the article*).

The absorption peaks at a wavelength of 250 nm to 280 nm indicate an electronic transition from benzene and its derivatives, including various aromatic compounds, such as phenolics, which are contained in CJO [31]. Furthermore, these phenolic compounds in the C-dots/CJO composite may also act as an additional surface state of the C-dots.

The IR spectra of the C-dots, CJO, and C-dots/CJO samples are shown in Fig. (**7**). It can be observed in Fig. (**7**) that the C-dots/CJO composite spectrum is similar to the CJO spectrum in the region of 400 cm^{-1} to 1500 cm^{-1}. On the other hand, the region of 1500 cm^{-1} to 4000 cm^{-1} of the C-dots/CJO composite spectrum is similar to the C-dots spectrum. This means that the IR spectrum of the C-dots/CJO composite is a combination of the IR spectra of the C-dots and CJO. In the IR spectrum of CJO, the functional groups of O-H, -CH_2, C=O, -CH_3, and C-O are detected. The –CH_2 bond is one of the constituents of limonene compounds, while the -CH_3 bond represents linalool, cineol, and pinene compounds [32]. On the other hand, C-dots/CJO composite contains functional groups of O-H at 3423.30 cm^{-1}, C-H at 2069.35 cm^{-1}, C=C at 1637.39 cm^{-1}, and also -CH_3 and C-O. The C=C bonds identified in the C-dots/CJO composite show the existence of the C-dots, while the -CH_3 and C-O bonds are CJO compounds, which form the surface state of the C-dots.

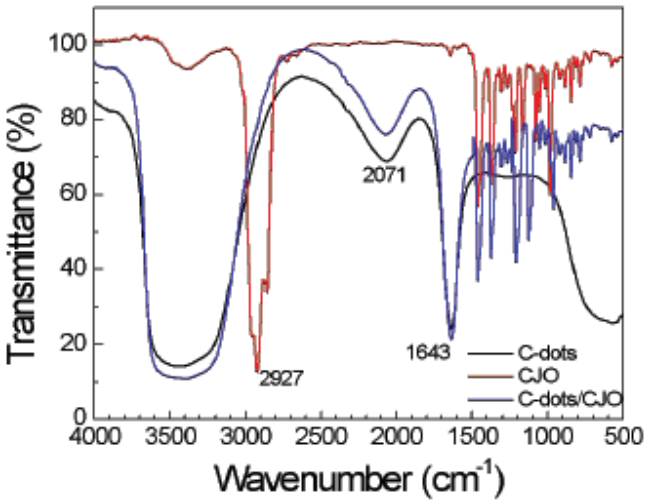

Fig. (7). IR spectra of the C-dots, CJO, and C-dots/CJO. (*A higher resolution / colour version of this figure is available in the electronic copy of the article*).

In order to investigate the antibacterial property of the C-dots/CJO composite, the antibacterial test was conducted. The measurement of the antibacterial activity of C-dots, CJO, and C-dots/CJO samples was performed using the diffusion method. The images of the DIZ for each sample are shown in Fig. (**8**). The white cloud-like substance covering most of the petri dishes in Figs. (**8a-8c**) is the *E. coli* colony. The DIZ is the area where the *E. coli* bacteria cannot penetrate the paper discs. It can be observed that all samples showed inhibition zones with different values of DIZ.

Furthermore, the DIZ values also differ depending on the illumination treatment, as can be observed in Table **1**. In the treatment without light (in the dark), the DIZ values produced by the C-dots, CJO, and C-dots/CJO samples were 1.83 mm, 3.03 mm, and 2.00 mm, respectively (Fig. **8a**). Afterward, under the white light treatment, the DIZ values produced by the samples (in the same order) were 1.87 mm, 2.23 mm, and 3.60 mm, respectively. Finally, under UV/violet light treatment, the DIZ values produced by the samples were 2.07 mm, 2.4 mm, and 2.73 mm, respectively. In the treatment without light, the highest DIZ value was achieved for CJO, while in the white light and UV/violet treatments, the C-dots/CJO composite had the highest DIZ value. Under the condition of no light, CJO was found to contain more antibacterial organic compounds, increasing its antibacterial activity. Exposing white light and UV/violet light to the C-dots and C-dots/CJO composite made the samples more active because of the photodynamic effect; hence, they exhibited higher antibacterial activities [19,33]. For each treatment, except for under no light conditions, the C-dots/CJO composite showed the highest DIZ value, indicating that the addition of CJO increased the antibacterial activity of C-dots. However, the DIZ category produced by each sample is still classified as having low response [34], as the preparation of the composite is not optimized.

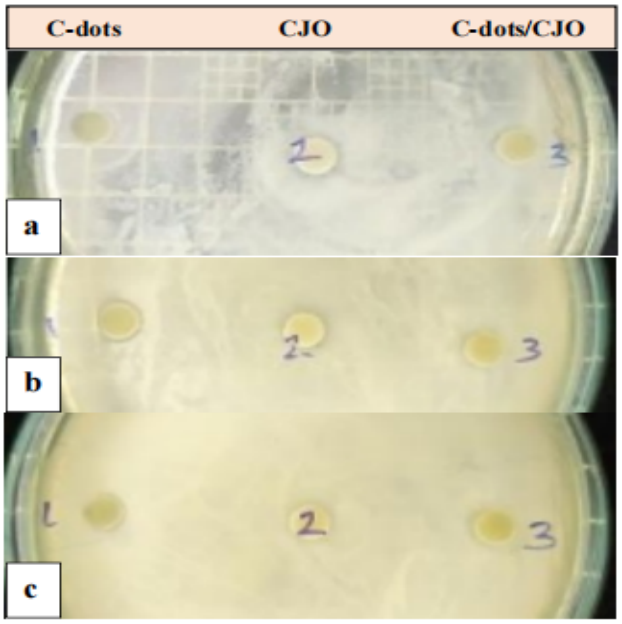

Fig. (8). Antibacterial activities of C-dots, CJO, and C-dots/CJO composite exposed to no light (a), white light (b), and UV/violet light (c) against *E. coli* bacteria. (*A higher resolution / colour version of this figure is available in the electronic copy of the article*).

C-dots prepared from watermelon and pomegranate peels, *i.e.*, W-Cdots and P-Cdots, respectively, displayed DIZ values of 12 mm and 14 mm, respectively, against *E. coli* at a volume of 5 µL. At a volume of 80 µL, the resulting DIZ values of W-Cdots and P-Cdots reached 19 mm and 24 mm, respectively [35]. On the other hand, the C-dots prepared from *Gum Arabic* (GA) exhibited a DIZ value of 1.1 mm against *E. coli* [17]. The C-dots were then conjugated

Table 1. The DIZ of the samples against *E. coli*.

Material	DIZ Under Various Light Sources (mm)			Antibacterial Response [34]
	Without Light (Dark)	White Light	UV/Violet Light	
C-dots	1.83	1.87	2.07	Low
CJO	3.03	2.23	2.40	
C-dots/CJO	2.00	3.60	2.73	

Table 2. DIZ comparison of various C-dots samples.

Material		DIZ (mm)	References
C-dots Under UV/Violet Light		2.07	Current Study
C-dots/CJO Under White Light		3.60	
W-Cdots	(5 µL)	12.0	[35]
	(80 µL)	19.0	
P-Cdots	(5 µL)	14.0	
	(80 µL)	24.0	
C-dots from GA		1.00	[17]
C-dots/ciprofloxacin		2.50	
Ciprofloxacin		2.60	

with ciprofloxacin, which increased the DIZ value to 2.5 mm, while the pure ciprofloxacin displayed a DIZ value of 2.6 mm. Here, the highest DIZ value was shown by C-dots/CJO composite exposed to white light, *i.e*., 3.6 mm, which was higher than the DIZ of C-dots conjugated with ciprofloxacin but lower than the DIZs of W-Cdots and P-Cdots. The DIZ comparison of various C-dots samples can be observed in Table **2**.

Several known mechanisms are attributed to the antibacterial abilities of the samples in this study, *i.e*., membrane cell damage and photodynamic inactivation effect and/or photodisinfection (PD) [36-38]. For the condition of no light (dark), the antibacterial mechanism depends upon the ability of the samples to damage the membrane cell of the *E. coli* bacteria. In this study, C-dots, CJO, and C-dots/CJO particles disrupted the cytoplasmic membrane of the bacteria causing intracellular material losses [38]. Furthermore, the highest DIZ obtained by the C-dots/CJO composite could be attributed to the photodynamic effect and PD of the C-dots and CJO, respectively, working in a synergetic fashion when exposed to visible light. The visible light exposed to the C-dots and CJO caused photo-excitations. The redox pairs were produced after photo-excitation and contributed to killing bacterial cells by generating reactive oxygen species (ROS) [19]. Hence, the DIZ value of the C-dots/CJO composite was higher when exposed to white light. Moreover, the DIZ of the C-dots/CJO composite exposed to white light was found to be higher than the DIZ of the C-dots/CJO composite exposed to UV/violet light. This indicates that the whole spectrum of visible light contributed to the combined photodynamic effect and PD of the C-dots/CJO composite by producing more ROS than the UV/violet light alone.

CONCLUSION

C-dots and C-dots/CJO composite were successfully prepared from the wastes of the CJO distillation process. The resulting C-dots produced cyan luminescence with a decay lifetime of 6.54 ns. Based on the antibacterial tests, the DIZ value of the C-dots/CJO composite was higher than the pure C-dots. The C-dots/CJO composite reached the highest DIZ of 3.6 nm under white light. The antibacterial activities of the C-dots/CJO composite were observed to be more effective when exposed to white and UV/violet light treatments, which was attributed to the photodynamic effect and PD of the C-dots and CJO, respectively. Although the DIZ obtained in this study is categorized as a low response, the C-dots and C-dots/CJO composite can be antibacterial agents against *E. coli*. Hence, further studies should be conducted to optimize the volume ratio of the C-dots and CJO in the composite in order to produce optimum DIZ against *E. coli* bacteria. Another interesting study may be conducted by using varying bacteria being tested against the C-dots/CJO composite.

LIST OF ABBREVIATIONS

0D = Zero-dimensional

C-dots = Carbon Nanodots

CJO = Cajuput Oil

DI = Deionized Water

DIZ = Diameter of Inhibition Zone

FTIR = Fourier Transform Infrared

GA = *Gum Arabic*

GQDs = Graphene Quantum Dots

HOMO = Highest Occupied Molecular Orbital

HRTEM = High-Resolution Transmission Electron Microscope

IR = Infrared

LED = Light Emitting Diode

MRSA = Methicillin-resistant *Staphylococcus aureus*

NA = Nutrient Agar

NB = Nutrient Broth

P-Cdots = Pomegranate Carbon Nanodots

PL = Photoluminescence

TRPL = Time-resolved Photoluminescence

UV = Ultraviolet

UV-Vis = Ultraviolet-visible

VRE = Vancomycin-resistant *Enterococcus faecium*

W-Cdots = Watermelon Carbon Nanodots

P-Cdots = Pomegranate Carbon Nanodots

ETHICS APPROVAL AND CONSENT TO PARTICIPATE

Not applicable.

HUMAN AND ANIMAL RIGHTS

No animals/humans were used that are basis of this study.

CONSENT FOR PUBLICATION

Not applicable.

AVAILABILITY OF DATA AND MATERIALS

Not applicable.

FUNDING

This study is financially supported by the International Collaboration Research Grant under contract number B/25/UN34.13/CRG.01.03/2020.

CONFLICT OF INTEREST

The authors declare no conflict of interest, financial or otherwise.

ACKNOWLEDGEMENTS

The authors would like to thank the Universitas Negeri Yogyakarta for funding this study through the International Collaboration Research Grant under contract number B/25/UN34.13/CRG.01.03/2020.

REFERENCES

[1] Cacciatore, FA; Brandelli, A; Malheiros, PS Combining natural antimicrobials and nanotechnology for disinfecting food surfaces and control microbial biofilm formation. *Crit Rev Food Sci Nutr,* **2020**, *61*(22), 3771-3782. http://dx.doi.org/10.1080/10408398.2020.1806782

[2] Wang, J.; Fan, H.; He, X.; Zhang, F.; Xiao, J.; Yan, Z.; Feng, J.; Li, R. Response of bacterial communities to variation in water quality and physicochemical conditions in a river-reservoir system. *Glob. Ecol. Conserv.,* **2021**, *27*, e01541. http://dx.doi.org/10.1016/j.gecco.2021.e01541

[3] Dong, X.; Awak, M.A.; Tomlinson, N.; Tang, Y.; Sun, Y.P.; Yang, L. Antibacterial effects of carbon dots in combination with other antimicrobial reagents. *PLoS One,* **2017**, *12*(9), e0185324. http://dx.doi.org/10.1371/journal.pone.0185324 PMID: 28934346

[4] Dong, X.; Liang, W.; Meziani, M.J.; Sun, Y.P.; Yang, L. Carbon dots as potent antimicrobial agents. *Theranostics,* **2020**, *10*(2), 671-686. http://dx.doi.org/10.7150/thno.39863 PMID: 31903144

[5] Sun, H.; Gao, N.; Dong, K.; Ren, J.; Qu, X. Graphene quantum dots-band-aids used for wound disinfection. *ACS Nano,* **2014**, *8*(6), 6202-6210. http://dx.doi.org/10.1021/nn501640q PMID: 24870970

[6] Yang, J.; Zhang, X.; Ma, Y.H.; Gao, G.; Chen, X.; Jia, H.R.; Li, Y.H.; Chen, Z.; Wu, F.G. Carbon dot-based platform for simultaneous bacterial distinguishment and antibacterial applications. *ACS Appl. Mater. Interfaces,* **2016**, *8*(47), 32170-32181. http://dx.doi.org/10.1021/acsami.6b10398 PMID: 27786440

[7] Liu, W.; Li, C.; Sun, X.; Pan, W.; Yu, G.; Wang, J. Highly crystalline carbon dots from fresh tomato: UV emission and quantum confinement. *Nanotechnology,* **2017**, *28*(48), 485705. http://dx.doi.org/10.1088/1361-6528/aa900b PMID: 28961145

[8] Peng, Z.; Han, X.; Li, S.; Al-Youbi, A.O.; Bashammakh, A.S.; El-Shahawi, M.S.; Leblanc, R.M. Carbon dots: Biomacromolecule interaction, bioimaging and nanomedicine. *Coord. Chem. Rev.,* **2017**, *343*, 256-277. http://dx.doi.org/10.1016/j.ccr.2017.06.001

[9] Xia, C.; Zhu, S.; Feng, T.; Yang, M.; Yang, B. Evolution and synthesis of carbon dots: From carbon dots to carbonized polymer dots. *Adv. Sci.,* **2019**, *6*(23), 1901316. http://dx.doi.org/10.1002/advs.201901316 PMID: 31832313

[10] Phadke, C.; Mewada, A.; Dharmatti, R.; Thakur, M.; Pandey, S.; Sharon, M. Biogenic synthesis of fluorescent carbon dots at ambient temperature using *Azadirachta indica* (Neem) gum. *J. Fluoresc.,* **2015**, *25*(4), 1103-1107. http://dx.doi.org/10.1007/s10895-015-1598-x PMID: 26123675

[11] Dwandaru, W.S.B.; Bilqis, S.M.; Wisnuwijaya, R.I.; Isnaeni, Optical properties comparison of carbon nanodots synthesized from commercial granulated sugar using hydrothermal method and microwave. *Mater. Res. Express,* **2019**, *6*(10), 105041. http://dx.doi.org/10.1088/2053-1591/ab3952

[12] Hou, Y.; Lu, Q.; Deng, J.; Li, H.; Zhang, Y. One-pot electrochemical synthesis of functionalized fluorescent carbon dots and their selective sensing for mercury ion. *Anal. Chim. Acta,* **2015**, *866*, 69-74. http://dx.doi.org/10.1016/j.aca.2015.01.039 PMID: 25732694

[13] Deng, J.; Lu, Q.; Mi, N.; Li, H.; Liu, M.; Xu, M.; Tan, L.; Xie, Q.; Zhang, Y.; Yao, S. Electrochemical synthesis of carbon nanodots directly from alcohols. *Chemistry,* **2014**, *20*(17), 4993-4999. http://dx.doi.org/10.1002/chem.201304869 PMID: 24623706

[14] Ang, W.L.; Boon, M.C.A.L.; Sambudi, N.S.; Mohammad, A.W.; Leo, C.P.; Mahmoudi, E.; Ba-Abbad, M.; Benamor, A. Microwave-assisted conversion of palm kernel shell biomass waste to photoluminescent carbon dots. *Sci. Rep.,* **2020**, *10*(1), 21199. http://dx.doi.org/10.1038/s41598-020-78322-1 PMID: 33273663

[15] Zhou, J.; Sheng, Z.; Han, H.; Zou, M.; Li, C. Facile synthesis of fluorescent carbon dots using watermelon peel as a carbon source. *Mater. Lett.,* **2012**, *66*(1), 222-224. http://dx.doi.org/10.1016/j.matlet.2011.08.081

[16] Li, L.; Zhang, R.; Lu, C.; Sun, J.; Wang, L.; Qu, B.; Li, T.; Liu, Y.; Li, S. *In situ* synthesis of NIR-light emitting carbon dots derived from spinach for bio-imaging applications. *J. Mater. Chem. B Mater. Biol. Med.,* **2017**, *5*(35), 7328-7334. http://dx.doi.org/10.1039/C7TB00634A PMID: 32264182

[17] Thakur, M.; Pandey, S.; Mewada, A.; Patil, V.; Khade, M.; Goshi, E.; Sharon, M. Antibiotic conjugated fluorescent carbon dots as a theranostic agent for controlled drug release, bioimaging, and enhanced antimicrobial activity. *J. Drug Deliv.,* **2014**, *2014*, 282193. http://dx.doi.org/10.1155/2014/282193 PMID: 24744921

[18] Kumar, V.B.; Natan, M.; Jacobi, G.; Porat, Z.; Banin, E.; Gedanken, A. Ga@C-dots as an antibacterial agent for the eradication of *Pseudomonas aeruginosa. Int. J. Nanomed.,* **2017**, *12*, 725-730. http://dx.doi.org/10.2147/IJN.S116150 PMID: 28176980

[19] Abu, R.D.I.; Mohammed, O.O.; Dong, X.; Patel, A.K.; Overton, C.M.; Tang, Y.; Kathariou, S.; Sun, Y.P.; Yang, L. Carbon dots for highly effective photodynamic inactivation of multidrug-resistant bacteria. *Mater. Adv.,* **2020**, *1*(3), 321-325. http://dx.doi.org/10.1039/D0MA00078G

[20] Pham, J.V.; Yilma, M.A.; Feliz, A.; Majid, M.T.; Maffetone, N.; Walker, J.R.; Kim, E.; Cho, H.J.; Reynolds, J.M.; Song, M.C.; Park, S.R.; Yoon, Y.J. A review of the microbial production of bioactive natural products and biologics. *Front. Microbiol.,* **2019**, *10*, 1404. http://dx.doi.org/10.3389/fmicb.2019.01404 PMID: 31281299

[21] Musta, R.; Nurliana, L.; Damhuri,; Asranudin,; Darlian, L.; Rudi, L. Kinetics study of antibacterial activity of Cajuput oil (*Melaleuca cajuputi*) on *Eschericia coli, Staphylococcus*, and *Bacillus cereus*. *Curr. Appl. Sci. Technol.,* **2021**, *22*(3), 3. http://dx.doi.org/10.55003/cast.2022.03.22.002

[22] Chaudhari, A.K.; Singh, V.K.; Das, S.; Kujur, A.; Deepika, ; Dubey, N.K. Unveiling the cellular and molecular mode of action of *Melaleuca cajuputi* Powell. essential oil against aflatoxigenic strains of *Aspergillus flavus* isolated from stored maize samples. *Food Control,* **2022**, *138*, 109000. http://dx.doi.org/10.1016/j.foodcont.2022.109000

[23] Desdiani, D.; Fadilah, F.; Sutarto, A.P. The effects of melaleuca cajuput oil (*Melaleuca cajuputi*) herbal treatment on clinical, laboratory, and radiological improvement and length of hospital stay in COVID-19 patients. *J. Appl. Pharm. Sci.,* **2022**, *12*(06), 122-127. http://dx.doi.org/10.7324/JAPS.2022.120611

[24] Chiocchio, I.; Mandrone, M.; Tomasi, P.; Marincich, L.; Poli, F. Plant secondary metabolites: an opportunity for circular economy. *Molecules,* **2021**, *26*(2), 495. http://dx.doi.org/10.3390/molecules26020495 PMID: 33477709

[25] Wu, Z.L.; Liu, Z.X.; Yuan, Y.H. Carbon dots: materials, synthesis, properties and approaches to long-wavelength and multicolor emission. *J. Mater. Chem. B Mater. Biol. Med.,* **2017**, *5*(21), 3794-3809. http://dx.doi.org/10.1039/C7TB00363C PMID: 32264241

[26] Dwandaru, W.S.B.; Fadli, A.L.; Sari, E.K. Cdots and Cdots/S synthesis from Nam-nam fruit (*Cyanometra cauliflora* L.) *via* frying method using cooking oil. *Dig. J. Nanomater. Biostruct.,* **2020**, *15*(2), 555-560.

[27] Isnaeni, I.; Suliyanti, M.M.; Shiddiq, M. Optical properties of toluene-soluble carbon dots prepared from laser-ablated coconut fiber. *Makara J. Sci.,* **2019**, *23*(4), 187-192. http://dx.doi.org/10.7454/mss.v23i4.10639

[28] Mewada, A.; Pandey, S.; Shinde, S.; Mishra, N.; Oza, G.; Thakur, M.; Sharon, M.; Sharon, M. Green synthesis of biocompatible carbon dots using aqueous extract of *Trapa bispinosa* peel. *Mater. Sci. Eng. C,* **2013**, *33*(5), 2914-2917. http://dx.doi.org/10.1016/j.msec.2013.03.018 PMID: 23623114

[29] Fan, T.; Zeng, W.; Tang, W.; Yuan, C.; Tong, S.; Cai, K.; Liu, Y.; Huang, W.; Min, Y.; Epstein, A.J. Controllable size-selective method to prepare graphene quantum dots from graphene oxide. *Nanoscale Res. Lett.,* **2015**, *10*(1), 55. http://dx.doi.org/10.1186/s11671-015-0783-9 PMID: 25852352

[30] Bao, L.; Liu, C.; Zhang, Z.L.; Pang, D.W. Photoluminescence-tunable carbon nanodots: Surface-state energy-gap tuning. *Adv. Mater.,* **2015**, *27*(10), 1663-1667. http://dx.doi.org/10.1002/adma.201405070 PMID: 25589141

[31] Pretsch, E.; Buhlmann, P.; Affolter, C. *Structure and Determination of Organic Compounds (Tables of spectral data)*; Springer-Verlag: Berlin, **2000**. http://dx.doi.org/10.1007/978-3-662-04201-4

[32] Gualdron, A.F.; Becerra, E.N.; Pena, D.Y. Inhibitory effect of *Eucalyptus* and *Lippia Alba* essential oils on the corrosion of mild steel in hydrochloric acid. *J. Mater. Environ. Sci.,* **2013**, *4*, 143-158. https://www.jmaterenvironsci.com/Document/vol4/19-JMES-353-2013-Gualdron.pdf

[33] Sattarahmady, N.; Rezaie, Y.M.; Tondro, G.H.; Akbari, N. Bactericidal laser ablation of carbon dots: An *in vitro* study on wild-type and antibiotic-resistant *Staphylococcus aureus*. *J. Photochem. Photobiol. B,* **2017**, *166*, 323-332. http://dx.doi.org/10.1016/j.jphotobiol.2016.12.006 PMID: 28024283

[34] Elgayyar, M.; Draughon, F.A.; Golden, D.A.; Mount, J.R. Antimicrobial activity of essential oils from plants against selected pathogenic and saprophytic microorganisms. *J. Food Prot.,* **2001**, *64*(7), 1019-1024. http://dx.doi.org/10.4315/0362-028X-64.7.1019 PMID: 11456186

[35] Muktha, H.; Sharath, R.; Kottam, N.; Smrithi, S.P.; Samrat, K.; Ankitha, P. Green synthesis of carbon dots and evaluation of its pharmacological activities. *Bionanoscience,* **2020**, *10*(3), 731-744. http://dx.doi.org/10.1007/s12668-020-00741-1

[36] Wu, X.; Abbas, K.; Yang, Y.; Li, Z.; Tedesco, A.C.; Bi, H. Photodynamic anti-bacteria by carbon dots and their nano-composites. *Pharmaceuticals,* **2022**, *15*(4), 487. http://dx.doi.org/10.3390/ph15040487 PMID: 35455484

[37] Li, Z.H.; Cai, M.; Liu, Y.S.; Sun, P.L.; Luo, S.L. Antibacterial activity and mechanisms of essential oil from *Citrus medica* L. var. sarcodactylis. *Molecules,* **2019**, *24*(8), 1577. http://dx.doi.org/10.3390/molecules24081577 PMID: 31013583

[38] Marqués, C.M.S.; Codony, F.; Agustí, G.; Lahera, C. Visible light enhances the antimicrobial effect of some essential oils. *Photodiagn. Photodyn. Ther.,* **2017**, *17*, 180-184. http://dx.doi.org/10.1016/j.pdpdt.2016.12.002 PMID: 27965057